Materials Today Bio 30 (2025) 101380

Contents lists available at ScienceDirect

Materials Today Bio

journal homepage: www.journals.elsevier.com/materials-today-bio

An injectable shape-adaptive hydrogel system for subconjunctival injuries: *In situ* and permanently releases rapamycin to prevent fibrosis *via* promoting autophagy

Xue Sun [1], Haohao Cui [1], Jingfan Li, Boyuan An, Ruixing Liu, Zhihua Guo, Dandan Chu, Xingchen Geng, Bingbing Cui, Lei Zhu, Jingguo Li [*], Zhanrong Li [**]

Henan Eye Hospital, Henan Provincial People's Hospital, People's Hospital of Zhengzhou University, Zhengzhou, 450003, China

ARTICLE INFO

Keywords:
Subconjunctival fibrosis
Rapamycin
In situ hydrogel
Autophagy

ABSTRACT

Subconjunctival fibrosis (SCF) is a common and refractory eye disease that is a serious threat to vision. The severe side effects of existing drugs and low drug bioavailability due to the ocular barrier are major challenges in SCF treatment. Hence, there is an urgent need to explore safer and more effective strategies for administering anti-SCF drugs. Herein, an injectable and adaptable hydrogel system containing the antifibrotic drug rapamycin was fabricated to address this complex need. This system possesses moderate mechanical properties, self-healing and shape-adaptive capabilities, injectability, and biosafety. It is designed to promote autophagy by modulating the PI3K/AKT/mTOR/WIPI2 pathway, thereby inhibiting SCF. *In vivo* experiments utilizing a rat subconjunctival injury model indicated that *in situ* administration of this hydrogel system effectively inhibited SCF. This system constitutes a promising method for promoting autophagy to protect against SCF, which will foster its widespread application for other fibrotic diseases.

1. Introduction

Subconjunctival fibrosis (SCF), with a relatively high incidence, can arise from conditions such as chronic conjunctivitis, severe dry eye syndrome, and ocular trauma. It leads to several complications including symblepharon, recurrent pterygium, and poor outcomes in glaucoma filtration surgery, thereby impairing visual acuity. SCF involves a multistage wound healing process, where conjunctival fibroblasts differentiate into myofibroblasts, migrating and synthesizing extracellular matrix (ECM), causing excessive scarring [1]. The transforming growth factor-β1 (TGF-β1)/Smad2/3 pathway plays a crucial role in this process by inducing fibroblast-to-myofibroblast transition, which is regulated by autophagy [2].

Autophagy, an evolutionarily conserved lysosomal degradation pathway, regulates fibrosis by modulating TGF-β1 expression through proteolytic degradation. Studies show that inhibiting the TGF-β1/Smad pathway through autophagy activation may reduce fibrosis in organs such as the liver, while autophagy inhibition increases TGF-β1 levels, promoting renal and pulmonary fibrosis [3–5]. We previously showed that activating autophagy can inhibit the TGF-β1/Smad2/3 pathway, thereby alleviating SCF [6]. Collectively, this evidence demonstrates that targeting autophagy can be used as a therapeutic strategy to prevent SCF.

Currently, glucocorticoids, non-steroidal anti-inflammatory drugs (NSAIDs), and antiproliferative agents, such as mitomycin C (MMC) and 5-fluorouracil (5-FU), are extensively employed in the management of SCF. Glucocorticoids and NSAIDs are generally administered as topical eye drops, yet their therapeutic efficacy is substantially limited by the ocular barrier, resulting in low bioavailability [7]. Prolonged use of glucocorticoids is associated with significant adverse effects, including cataract, glaucoma, and an elevated risk of ocular infections, whereas NSAIDs are known to cause ocular irritation and corneal damage [8]. While intraoperative application of MMC bypasses the ocular barrier, its cytotoxicity can lead to severe complications, including scleral melting and corneal epithelial toxicity. Postoperative subconjunctival injections of 5-FU are rapidly metabolized, necessitating multiple invasive

* Corresponding author.
** Corresponding author.
E-mail addresses: lijingguo@zzu.edu.cn (J. Li), lizhanrong@zzu.edu.cn (Z. Li).
[1] These authors contributed equally to this work.

https://doi.org/10.1016/j.mtbio.2024.101380
Received 25 June 2024; Received in revised form 27 October 2024; Accepted 4 December 2024
Available online 10 December 2024

injections with limited efficacy [10]. These limitations underscore the urgent need for the development of safe and effective antifibrotic therapies. To address these issues, this study aims to design and fabricate an adaptive, drug-loaded hydrogel for controlled and sustained drug release. This hydrogel is intended for intraoperative implantation in the subconjunctival space, thereby overcoming the challenges of ocular drug delivery barriers and ensuring localized, prolonged release of the therapeutic agent at the target site. The hydrogel system will be evaluated for its antifibrotic efficacy, underlying mechanisms of action, and biosafety profile.

Rapamycin (RAP) can regulate the activity of Unc-51-like autophagy activating kinase 1 (ULK1) in the initial step of autophagosome formation by controlling the mammalian target of rapamycin complex 1 (mTORC1) [11]. Research has demonstrated that RAP exhibits antifibrotic properties in both renal and pulmonary tissues, positioning it as a potential candidate for autophagy regulation and SCF inhibition [12,13]. Despite this, its clinical application remains constrained due to its poor water solubility [14]. Moreover, drug delivery *via* eye drops faces significant challenges, including low bioavailability (<5 %) caused by the tear film and blood-eye barriers, as well as the lipophilic nature of the conjunctival epithelium, which limits drug penetration and reduces residence time, necessitating frequent administration [15,16]. Hence, overcoming these formidable obstacles and delivering RAP to the subconjunctival tissue poses a monumental challenge. In subconjunctival injury models, if a sustained release system is directly applied to the site of injury, barrier effects can be bypassed, thereby achieving controlled and prolonged action of RAP at the target site. The fabrication of novel biomaterial-based drug delivery systems is imperative for increasing bioavailability and achieving therapeutic efficacy.

Hydrogels are an emerging class of biocompatible scaffolds that are promising biomaterials for tissue engineering and drug therapies. Functionalized hydrogels are a novel and emerging research focus. Hydrogels have ECM-like characteristics and have been employed in wound care, hemostatic sealing, and drug delivery. [17,18] These gels may prevent excessive collagen deposition and alleviate scar formation [19,20]. Moreover, gel drug delivery systems have been demonstrated to allow the increased retention and permanent *in situ* release of drugs to improve trauma management [21,22]. In addition, the integrity of self-healing hydrogels can be spontaneously restored upon damage. Rational dynamic gel designs ensure excellent injectability, allowing the filling of deep irregularities and preventing uneven administration [23–27]. Hence, a hydrogel drug delivery system is the optimal choice for achieving *in situ* drug delivery and long-term release.

Subconjunctival injection gels include thermosensitive hydrogels like poly(lactic-co-glycolic acid)-b-poly(ethylene glycol)-b-poly(lactic-co-glycolic acid) (PLGA-PEG-PLGA), thiol-ene click hydrogels, photopolymerized carbon-carbon double-bond hydrogels, etc. [28–32] However, they have certain drawbacks, such as the weak mechanical strength of PLGA−PEG−PLGA, the difficulty in preserving mercaptans, and the irritation caused by light. Considering their injectability and degradability, for this study, dynamic adaptive hydrogels were prepared by borate ester cross-linking. These hydrogels exhibit time-dependent drug release and gradual degradation, making them suitable for the treatment of chronic diseases.

To increase bioavailability and achieve therapeutic efficacy, a hydrogel-based drug delivery system was prepared in this work. The mechanical properties, self-healing ability, injectability, and safety of the hydrogel system were extensively investigated *in vitro*. The antifibrotic effects of RAP *in vitro* were investigated through proliferation, contraction, and migration assays. Moreover, the potential molecular pathways by which RAP promotes autophagy to inhibit fibrosis were identified through RNA sequencing (RNA-seq) analysis. The potential signaling pathways involved and their inhibitory effects on fibrosis were validated at multiple levels, including the cellular and translational levels. Finally, the inhibitory effect of the hydrogel system on SCF was verified by subconjunctival injection of a hydrogel loaded with RAP (CP/RAP).

2. Materials and methods

2.1. Materials

Chitosan (CS, 30 kDa) was obtained from Jinan Haide Beihai Marine Biotechnology Co., Ltd., China. β-Cyclodextrin (β-CD) was procured from Shanghai Aladdin Reagent Co., Ltd. Polyvinyl alcohol (PVA, Mw: 20 kDa) was procured from Jiangxi Alpha Industry Co., Ltd. N-Hydroxy succinimide (NHS) and 1-ethyl-3-(3′-dimethylaminopropyl) carbodiimide (EDC) were purchased from Beijing Bioway Biotech Company. 4-Carboxyphenylboronic acid (PBA) was obtained from J&K Scientific Ltd. (Beijing, China). RAP was acquired from Sigma−Aldrich. The Cell Counting Kit-8 (CCK-8) assay kit was obtained from Shanghai Liji Biotech Co., Ltd., and concurrently, the collagen contraction assay kit was sourced from Cell Biolabs, Inc. Anti-mTOR and anti-phospho-mTOR were procured from Cell Signaling Technology. In parallel, antibodies against phosphoinositide 3-kinase (PI3K), phospho-PI3K, protein kinase B 1 (AKT1), AKT1/2/3, phospho-AKT, fibrinogen (FN), TGF-β1, and smooth muscle alpha-actin (α-SMA) were purchased from Bioss. Moreover, antibodies against Beclin1, sequestosome-1 (SQSTM1/P62), WD repeat domain phosphoinositide interacting 2 (WIPI2), phospho-WIPI2, ribosomal protein S6 (RPS6), phospho-RPS6, light chain 3A (LC3A), light chain 3B (LC3B), DEP domain-containing mTOR-interacting protein (Deptor), Raptor and type I collagen (COL I) and type III collagen (COL III) were obtained from Affinity, and antibodies against HUWE1 were obtained from Abcam.

2.2. Preparation of β-CD-COOH

To prepare carboxymethyl-functionalized β-CD (β-CD-COOH), CS was reacted with sodium hydroxide. Specifically, β-CD (20 mmol) and sodium chloride (360 mmol) were dissolved in 30 mL of distilled water, after which an aqueous solution of sodium chloroacetate (20 mmol) was added dropwise to the β-CD solution under vigorous stirring at 50 °C for 7 h. The pH of the resulting solution was then adjusted to approximately 7 using HCl. Subsequently, the reaction mixture was precipitated in a 5-fold excess of an acetone-methanol mixed solvent and filtered. The resulting white powder was dried in a vacuum oven at 80 °C overnight for subsequent use. The successful synthesis of β-CD-COOH was confirmed *via* ^{1}H NMR and FTIR spectral analysis.

2.3. Synthesis of CS-g-CD (CC)

The CC was synthesized by grafting β-CD-COOH onto the amino groups of the chitosan backbone. Specifically, CS (1.668 g) was dissolved in distilled water at a concentration of 2 % (w/v). A solution containing β-CD-COOH (4 mmol), NHS (4 mmol), and EDC (4 mmol), at a molar ratio of chitosan amino groups to β-CD-COOH of approximately 5:2, was prepared in distilled water and stirred at room temperature for 2 h. This solution was then added dropwise to the CS solution, with stirring conditions maintained. Following the reaction, the mixture was transferred to a dialysis membrane (Mw = 3500 Da) and dialyzed for 48 h to remove unreacted reagents. The final product was stored at 4 °C until use. The grafting efficiency, as determined by ^{1}H NMR, was confirmed to be 40 %.

2.4. Preparation of cyclodextrin and phenylboronic acid (CCP)

PBA was mixed with NHS and EDC at a molar ratio of 1:1.5:1.5. This mixture was dissolved in anhydrous DMF with stirring for 2 h to obtain a homogeneous solution, which was then added to the CC solution to completely react with the remaining amino groups on the chitosan backbone. The resulting solution was subsequently dialyzed for 48 h to remove impurities. Excess PBA monomer was removed by

centrifugation, and the final product was freeze-dried and stored in a desiccator until use.

2.5. Preparation of CCP/RAP and CP/RAP

The RAP ethanol solution was introduced into the CCP solution (40 mg/mL) and stirred vigorously in the dark for 24 h, followed by dialysis to remove unbound RAP. The solution was then lyophilized, and the resulting solid was immersed in acetonitrile for a sufficiently long period. The supernatant was collected, diluted, and analyzed by high-performance liquid chromatography (HPLC). The standard curve was recorded as: $y = 7.95 \times 10^4 \times -4.07 \times 10^4$, $R^2 = 0.999$. A CCP/RAP solution (30 mg/mL) was then mixed with polyvinyl alcohol solutions at varying concentrations (5, 10, 15, or 20 mg/mL) to prepare the corresponding hydrogels.

2.6. Degradation of the CP hydrogel

Hydrogel samples (n = 3) were soaked in PBS for 24 h to achieve swelling equilibrium, weighed (recorded as M_0), and then placed in centrifuge tubes containing 10 mL of PBS (pH 7.4). The tubes were maintained at 37 °C with continuous shaking. At designated intervals, the mass (Mt) of the hydrogels was recorded, and the remaining mass percentage was calculated as:

$$\text{Remaining mass} = M_t/M_0 \times 100\%$$

2.7. Rheological measurements of the CP hydrogel

The rheological properties of the CP hydrogel were evaluated using a TA rheometer. Oscillatory frequency sweep tests were conducted to measure the storage modulus (G′) and loss modulus (G″) of the hydrogel following established protocols.

2.8. Self-healing behavior of the CP hydrogel

The self-healing properties of the CP hydrogel were assessed *via* rheological analysis and macroscopic autonomous healing tests. A strain sweep test was performed to identify the linear viscoelastic region and determine the fracture strain. The CP hydrogel was then bisected with a scalpel and reassembled at the cut interface. Its injectability was further evaluated by syringe injection tests.

2.9. Cell culture

Human pterygium specimens were obtained from surgical excisions performed at Henan Provincial People's Hospital, with ethical approval secured from the institutional review board. The pterygium tissues were immersed in a 10 % penicillin-streptomycin solution for 30 min and then carefully sectioned into 2 × 2 mm fragments under sterile conditions. These tissue fragments were subsequently cultured in 25 cm^2 flasks. To initiate cell culture, 0.5 mL of complete medium, composed of 90 % DMEM/F12 medium, 10 % Gibco serum, and 1 % penicillin-streptomycin solution, was added to each flask. The flasks were placed in a controlled incubator at 37 °C with 5 % CO_2 to promote cellular proliferation. Incubation continued until human pterygium fibroblasts (HPFs) proliferated from the tissues. HPFs from passages 2 to 5 were selectively used for further experiments.

2.10. Cell proliferation experiment

Three experimental groups were established: the CON group, the TGF-β1 group, and the RAP group (with concentrations of 0.5, 1, 2, 4, and 8 μg/mL). HPFs were seeded into 96-well plates at a density of 1×10^4 cells per well, with each well containing 100 μL of complete medium. Cells were incubated overnight at 37 °C under 5 % CO_2. In the RAP group, cells were pretreated with various concentrations of RAP for 24 h, followed by exposure to 10 ng/mL TGF-β1. The TGF-β1 group received TGF-β1 treatment alone, without prior drug pretreatment. CCK-8 solution (10 μL per 100 μL cell suspension) was added to each well, and after a 4-h incubation protected from light, absorbance at 450 nm was measured using a microplate reader. Cell proliferation activity was calculated, and each experiment was repeated at least three times to ensure data robustness and reproducibility.

2.11. Cell migration assay

This assay utilized the same groupings as the cell proliferation study. HPFs were seeded into six-well plates and cultured to approximately 90 % confluence. Cells in the RAP group were pretreated for 24 h, followed by 8 h of serum starvation in medium containing 0.5 % serum. A 200 μL pipette tip was used to scratch the cell monolayer in each well, and the cells were rinsed three times with PBS before being transferred to a serum-free medium supplemented with 10 ng/mL TGF-β1. At designated time points, the status of migrating cells was observed under a microscope, and the number of migrating cells was quantified.

2.12. Collagen contraction test

Cells were then harvested and resuspended at a concentration of 3×10^6 cells/mL. A collagen contraction working solution (composed of 2.385 mL collagen solution, 615 μL 5 × culture medium, and 85 μL neutralizing solution) was prepared on ice. The cell suspension was mixed with the cold collagen working solution at a 1:4 ratio and dispensed into a 12-well plate, then incubated for 1 h at 37 °C to allow for collagen polymerization. Afterward, 1 mL of culture medium was added, and the setup was cultured for two additional days. Following a 1-h pretreatment with 10 mM 2,3-butanedione monoxime (BDM), the collagen gels were gently released with a sterile scraper. Images of the collagen contraction at various time points were captured, and ImageJ software were used to calculate the collagen area and determine the relative collagen contraction rate.

2.13. RNA-seq analysis

Gene expression levels in HPFs induced by TGF-β1 with or without RAP were analyzed through RNA sequencing (RNA-seq). The CON, TGF-β1, and RAP groups were treated as described above. Triplicate samples of HPFs from each group were collected and stored at −80 °C for RNA-seq analysis by LC-Bio Technology Co., Ltd. (Hangzhou, China). Differentially expressed genes (DEGs) were identified by analyzing the transcriptomes of HPFs. Venn diagrams and a cluster heatmap of DEGs were generated using the web platform provided by LC-Bio Technology Co., Ltd. Kyoto Encyclopedia of Genes and Genomes (KEGG) pathway enrichment was conducted using the OmicStudio platform (https://www.omicstudio.cn/tool).

2.14. Immunofluorescence analysis

HPFs were seeded onto coverslips within six-well plates at a density of 5000 cells per well, with treatments aligned with the conditions previously established for the RAP and TGF-β1 groups. Following fixation with 4 % paraformaldehyde for 20 min, cells were rinsed with PBS. Membrane permeabilization was achieved through a 20-min incubation with 0.5 % Triton X-100, followed by a 30-min blocking step with goat serum after additional PBS washes. Subsequently, diluted primary antibodies were added, and the samples were incubated overnight at 4 °C. After washing, cells were incubated with fluorescein isothiocyanate (FITC) at room temperature for 1 h. Nuclei were counterstained using 4',6-diamidino-2-phenylindole (DAPI). Images were acquired using a research-grade immunofluorescence microscope, and fluorescence intensity was quantified using ImageJ.

2.15. Western blot

After cell processing, proteins were collected, and protein concentrations were determined *via* the BCA method. Equal amounts of protein samples were loaded onto a sodium dodecyl sulfate-polyacrylamide gel (SDS-PAGE) and then transferred onto a PVDF membrane. The membrane was blocked with 5 % skim milk for 1 h, followed by incubation with primary antibodies overnight at 4 °C. After washing with TBS-T, the membrane was incubated with HRP-conjugated anti-rabbit or anti-mouse secondary antibodies at room temperature for 1 h. Chemiluminescent reagents were applied to visualize the bands, and ImageJ was utilized to measure the grayscale values of the bands.

2.16. Animals

Eight-week-old female Sprague-Dawley (SD) rats (SPF grade), weighing 180–200 g, were obtained from Beijing Vital River Laboratory Animal Technology Co., Ltd. All experimental procedures adhered to the guidelines of the Experimental Animal Ethics Committee of Henan Eye Hospital (ethics number: HNEECA-2024-01).

2.17. Establishment of animal models

SD rats were randomly divided into the CON, blank hydrogel (CP), and drug-loaded hydrogel (CP/RAP) groups, with six rats in each group. Anesthesia was induced by intraperitoneal injection of 2 % pentobarbital sodium (2 mL/kg). The eyes and surrounding skin were disinfected with povidone-iodine. A corneal incision was made along the temporal margin, approximately one-third of the corneal circumference, and corneal scissors were used to separate the conjunctiva from the cornea. In the CP group and CP/RAP group, blank hydrogel and drug-loaded hydrogel were placed in the temporal conjunctival sac, respectively. Postoperative care included applying levofloxacin eye gel to the conjunctival sac. Tobramycin eye drops were administered to the operated eyes four times daily for one week to prevent infection. Quantitative scoring criteria for conjunctival congestion and edema severity were established (Table S1). Conjunctival edema and congestion were assessed at 2 and 8 weeks post-surgery, with photographic documentation using a slit lamp microscope.

2.18. Histologic evaluation and immunohistochemistry

Rat eye tissues were collected, fixed with FAS eye fixative, paraffin-embedded, and sectioned. Samples from 1, 2, and 8 weeks were stained with hematoxylin and eosin (H&E). Sections from 1 to 2 weeks were subjected to immunofluorescence staining for LC3A and LC3B. For samples at 8 weeks, immunofluorescence staining was conducted for COL I, COL III, and FN, and Masson's trichrome staining was performed.

2.19. Statistical analyses

Statistical analyses were conducted using GraphPad Prism 8.0. Results are presented as the mean ± standard deviation, with each experiment repeated at least three times. Statistical significance between groups was determined by one-way analysis of variance (ANOVA) followed by Bonferroni post-test. When data were hierarchical, the Kruskal-Wallis test was used. Statistical significance was set at $P < 0.05$.

3. Results and discussion

3.1. Preparation and characterization of hydrogel precursors

In this work, a grafted copolymer of CS conjugated to CCP was synthesized *via* a two-step carbodiimide coupling method as a vector for loading and solubilizing RAP *via* a host-guest supramolecular interaction with cyclodextrin. In this process, the phenylboronic acid group was employed to form a dynamic chemical bond with the diols of polyvinyl PVA, which acted as a crosslinking agent to fabricate a self-healing hydrogel system *via* borate esters for *in situ* and sustainable release of RAP for the treatment of SCF (Scheme 1).

All of the structural characteristics of the polymers were subsequently analyzed. Fig. 1A displays the ^{1}H NMR spectra of the polymers. The resonance peak at 4.9–5.0 ppm corresponded to the resonance of the cyclodextrin pyranose ring, the peak at 5.17 ppm was attributed to the characteristic peak of the introduced methylene hydrogen (-OCH_2-) after carboxylation, and the peak at 7.7–8.0 ppm was attributed to the benzene ring of the phenylboronic acid group. The peaks at 3.01 ppm and 1.9 ppm were attributed to the characteristic hydrogen resonance peaks of chitosan connected to the amino carbon and acetyl groups, respectively. By calculating the ratio of the integrated areas of the peaks at 5.17 ppm and 3.01 ppm in the CC spectrum, the degree of cyclodextrin grafting was determined to be 30 %. These results confirmed the successful synthesis of the polymeric carrier CCP. The precursors were synthesized in accordance with previously reported methods [33]. The FTIR spectra of PBA, CC, and CCP are shown in Fig. 1B. The peak at 1710 cm^{-1} was attributed to C=O, the peaks at 1525 and 1563 cm^{-1} were attributed to the phenyl ring skeleton (C-C), and the peak at 898 cm^{-1} were attributed to the chitosan β-pyranose ring, demonstrating that CCP may be the desired product. Fig. 1C presents the UV spectra of PVA, CC, and CCP, with the UV absorption peak at 240 nm confirming the conjugation of phenylboronic acid and chitosan. The hydrogel samples CP_1, CP_2, CP_3, and CP_4 were obtained by maintaining a constant CCP solution concentration of 3.5 % and adjusting the PVA solution concentration to 0.5 %, 1 %, 1.5 %, and 2 %, respectively, *via* equivalent mixing. CP_4/RAP is a RAP-loaded hydrogel. To observe more clearly whether the drug loading impaired the properties of the hydrogel, we compared the CP_4 hydrogel and CP_4-loaded drug hydrogel.

3.2. Physicochemical performance of the hydrogels

The mechanical properties of a hydrogel are highly important for its *in vivo* application as a hydrophilic three-dimensional network structure. Therefore, amplitude sweep tests and frequency sweep tests were first conducted to evaluate the performance of the hydrogels. As shown in Fig. 1D, the hydrogel underwent a gel–sol transition with increasing strain. With increasing angular frequency, the gel exhibited increased strength, a typical viscoelastic behavior induced by normal phenomena, indicating that the gel can withstand high-frequency motion without rupturing (Fig. 1E). To assess the effects of changes in the PVA content on the properties of the gels, we set the experimental conditions to a strain of 10 % and a frequency of 1 rad/s. Fig. 1F schematically shows the rheological properties of CP_1, CP_2, CP_3, and CP_4, indicating a gradual increase in gel strength with increasing PVA content, indicating increased internal crosslinking. Fig. 1G shows the changes in the mechanical properties of the gels before and after drug loading. The mechanical strength slightly increased after drug loading, an effect possibly related to the increase in hydrophobicity.

In the context of *in vivo* applications, the high-frequency motion of limbs under external loads may result in the rupture of the gel structure, influencing its therapeutic effectiveness. However, self-healing hydrogels can spontaneously recover their original form and function after experiencing external damage, a property that improves the material's safety profile. Consequently, a low strain of 10 % and a high strain of 250 % were selected as the alternating strain conditions for the self-healing experiments. As shown in Fig. 1H, under 250 % high-strain conditions, the hydrogel ruptured; however, the gel state was recovered under 10 % low-strain conditions and maintained for four cycles, demonstrating the self-healing capability of the material. The slight decrease in strength may be attributed to an insufficient recovery time. Subsequent shear viscosity tests were employed to evaluate the injectability of the gel (Fig. 1I). The results confirmed the injectable properties of the hydrogels from a microscopic perspective. Fig. 1J shows scanning

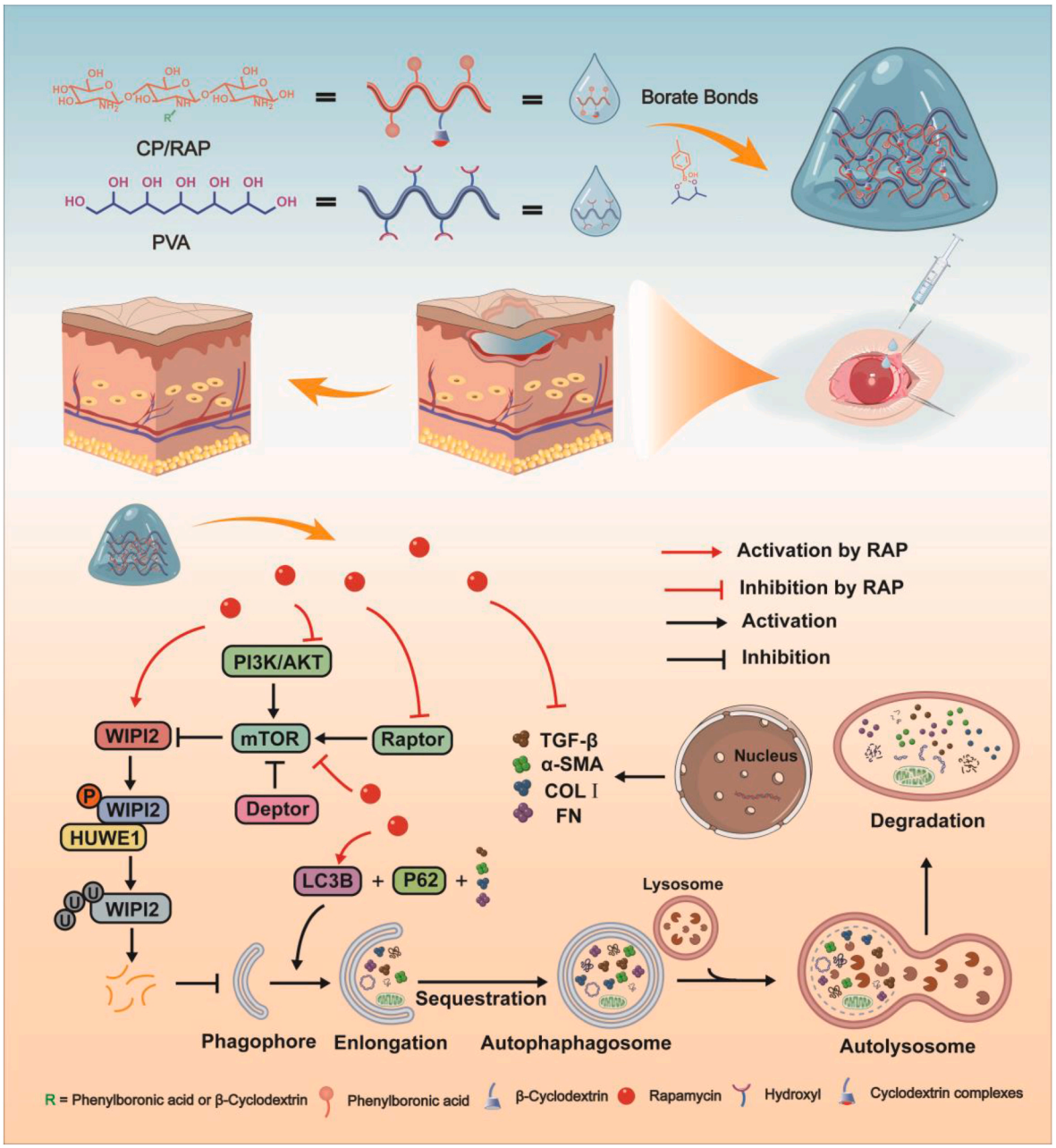

Scheme 1. Fabrication, treatment scheme, and molecular mechanism of the RAP-loaded adaptive gel.

electron microscopy (SEM) images of the various hydrogel groups. With increasing PVA content, the crosslinking density of the hydrogel increased, leading to a denser structure, which was consistent with the rheological test results.

Fig. 1K provides a schematic representation of macroscopic self-repair. The hydrogels were stained yellow and purple for clarity. Over time, the cracks at the interface of the differently colored hydrogels disappeared, and pigment diffusion at the interface was directly observable, confirming the exceptional self-repair properties of the hydrogels. CP_2 was chosen for the injection experiment because its PVA content of 1 % is consistent with the concentration of commercially available eye drops. Fig. 1L shows injection images of the CP_2 hydrogel, which can be injected through a 0.8 mm needle and molded into different shapes, underscoring the excellent writability of the material. While a higher crosslinking density implies greater strength and stability, it also renders injection more challenging.

The biodegradability of the hydrogels was also evaluated, and their quality tended to first decrease rapidly and then slowly. After 35 days, approximately 40 % of the mass remained (Fig. 1M). Borate bonds have been reported to be reactive oxygen species (ROS) sensitive; thus, we determined their radical scavenging capacity with 1,1-diphenyl-2-picrylhydrazyl (DPPH). The results revealed a slightly stronger free radical scavenging effect in the absence of a borate bond and a weaker ability after bond formation (Fig. 1N). Owing to its subsequent application convenience and the consistency of its PVA content with the concentration of commercially available eye drops, CP_2 was selected as the optimal material and was loaded with RAP for further experiments.

Good biosafety is a pivotal property for *in vivo* applications. Therefore, we assessed the viability of human fibroblasts cocultured with CP_2 hydrogels loaded with different concentrations of drugs. As shown in Fig. 1O, the viability of HPFs did not decrease significantly with increasing concentration, proving the blank hydrogels exhibited robust biosafety.

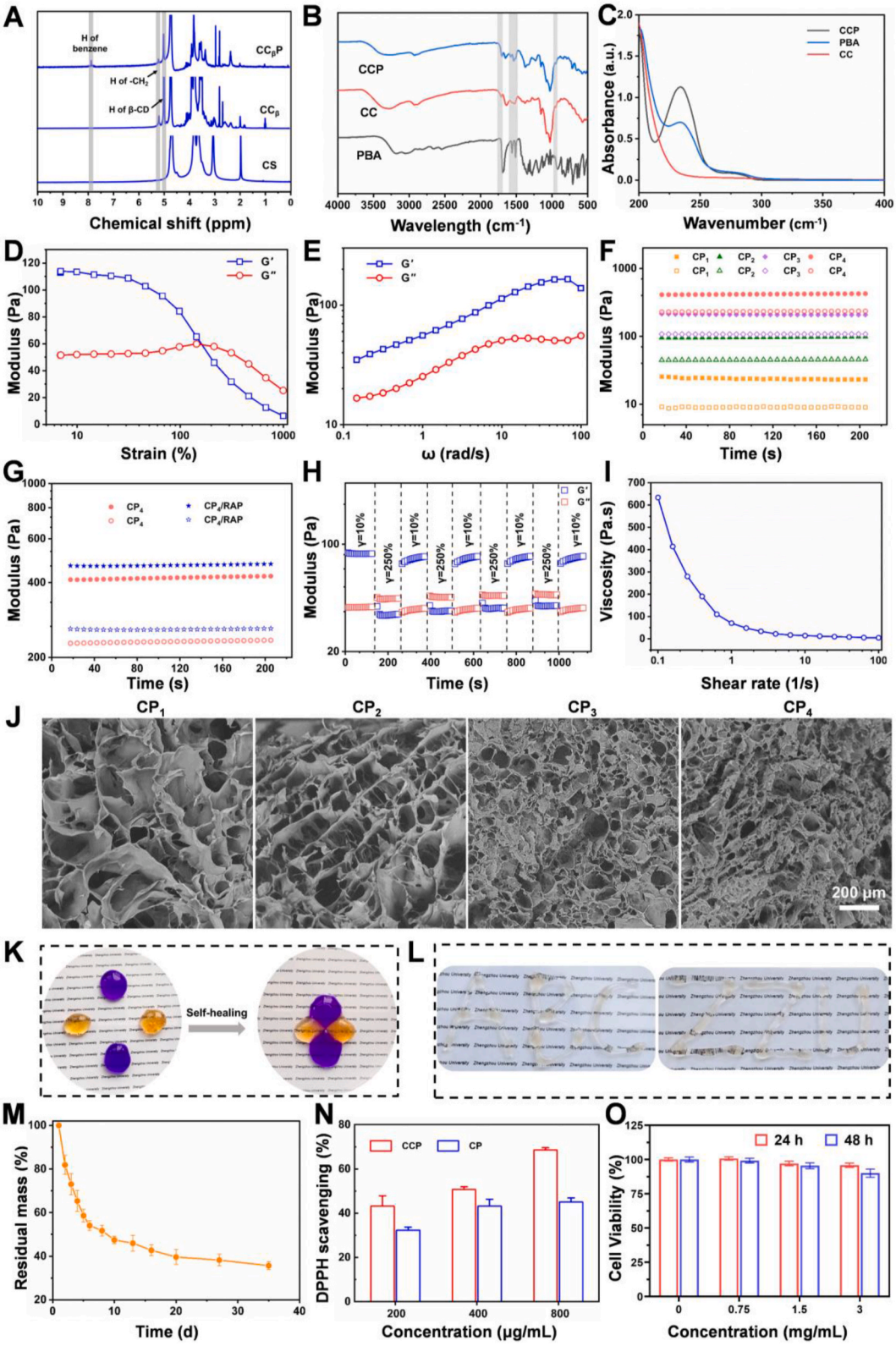

Fig. 1. Preparation and characterization of hydrogels. (A) ^{1}H NMR spectra of CS, CC, and CCP. (B) FTIR spectra of PVA, CC, and CCP. (C) UV–vis spectra of PVA, CC, and CCP. G′ and G″ in the (D) amplitude sweep test and (E) frequency sweep test at 32 °C. The CP_1, CP_2, CP_3, and CP_4 hydrogels consisted of CCP/RAP (30 mg/mL) and PVA (5, 10, 15, 20 mg/mL). (F) Rheological properties of the CP_1, CP_2, CP_3 and CP_4 hydrogels. (G) Rheological properties of hydrogels with or without RAP loading. (H) Alternating strain test of the CP_2 hydrogel. (I) Rheological profiles of the CP_2 hydrogel at 32 °C and shear rates of 0.1–100 s^{-1}. (J) SEM images of the CP_1, CP_2, CP_3, and CP_4 hydrogels. (K) Self-healing behavior of the hydrogels. (L) Optical injection image of the shear thinning characteristics. (M) Time-dependent degradation behavior of the CP_2 hydrogel (n = 3). (N) DPPH scavenging ability of CCP and CP (n = 3). (O) Cell viability of HPFs treated with different concentrations of CP after 24 h and 48 h (n = 3).

3.3. Inhibitory effects on the proliferation, contraction and migration of HPFs

Studies have indicated that TGF-β1 is a potent inducer of myofibroblast differentiation and activation, promoting the transformation of quiescent HPFs into myofibroblasts expressing α-SMA [34,35]. Therefore, inhibiting the activation and proliferation of myofibroblasts induced by TGF-β1 is crucial. Ki67, a proliferation-related antigen expressed in the nucleus, is a reliable marker of cell proliferation [36]. The percentage of Ki67-positive HPFs was increased after TGF-β1 treatment. RAP (0.5, 1.0 and 2.0 μg/mL) inhibited the expression of Ki67 in a concentration-dependent manner (Fig. 2A). There was no

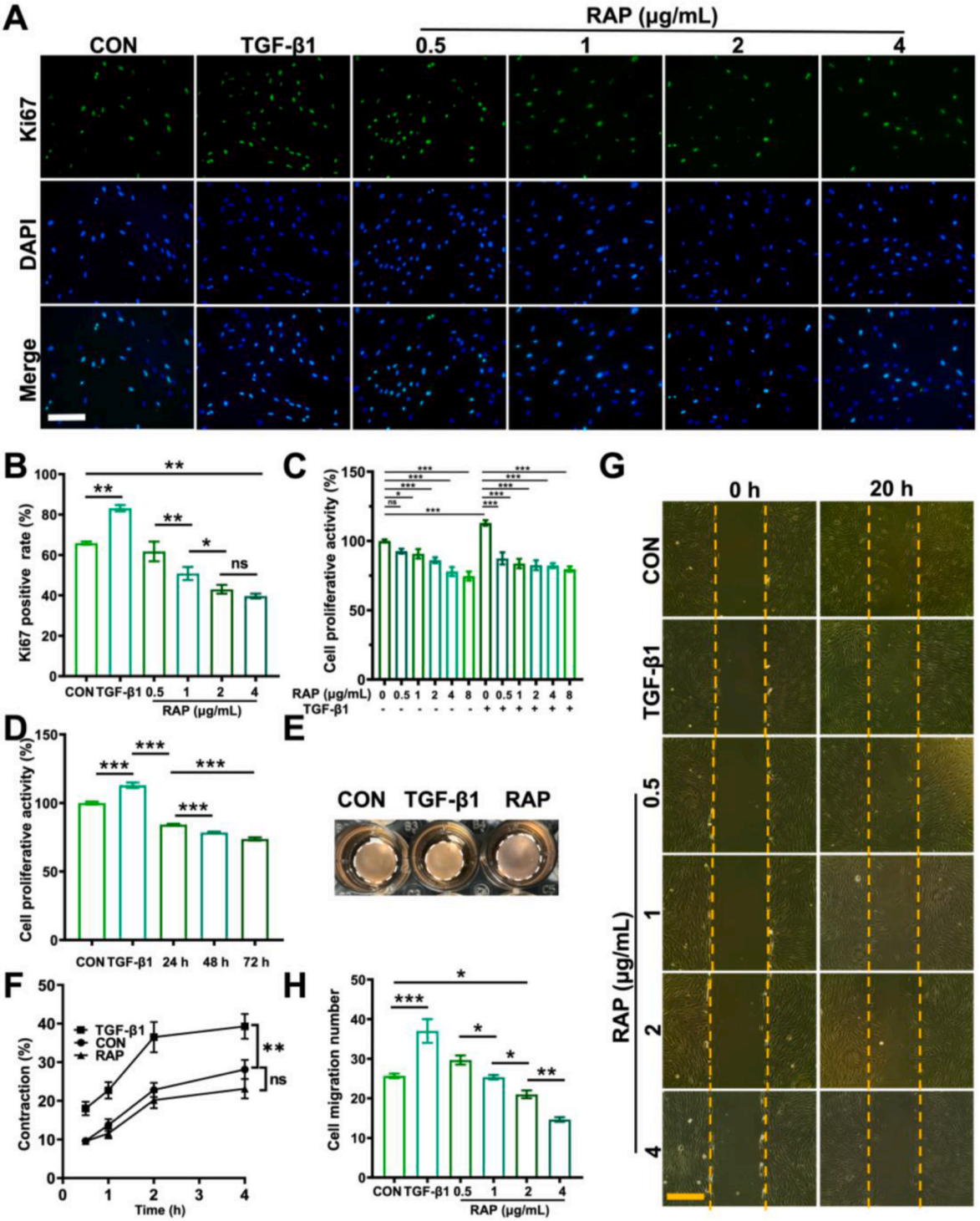

Fig. 2. RAP suppresses the proliferation, contraction and migration of HPFs. Ki67 expression (A) and positivity rate (n = 5) (B). Proliferation of HPFs after treatment with different concentrations of RAP for the same time (24 h) (C) or for different durations at the same concentration (2 μg/mL) (n = 5) (D). (E) Representative images of collagen contraction after 4 h, with the white dashed lines indicating the gel area (n = 5). (F) Relative area of gel contraction (%) at different times (n = 5). Images (G) and statistical analysis (H) of HPF migration (n = 5). *White scale bar*: 750 μm, *orange scale bar*: 150 μm $^{*}P < 0.05$, $^{**}P < 0.01$, $^{***}P < 0.001$. (For interpretation of the references to color in this figure legend, the reader is referred to the Web version of this article.)

statistically significant difference between the inhibitory effects of 2 μg/mL RAP and 4 μg/mL RAP on Ki67 expression (Fig. 2B). On the basis of the aforementioned results, 2 μg/mL was chosen for subsequent experiments. CCK-8 assays revealed that RAP effectively inhibited the proliferation of HPFs activated by TGF-β1. With increasing concentration, the inhibitory effect of RAP on cell proliferation became more pronounced (Fig. 2C). In addition, this inhibitory effect was time-dependent (Fig. 2D). These results indicate that RAP effectively suppresses the proliferation of HPFs activated by TGF-β1. The results in the CP/RAP group were consistent with those in the RAP group, in which TGF-β1 promoted cell viability and proliferation (Fig. S1).

Activated fibroblasts that mediate collagen contraction synthesize and secrete ECM components, which play important roles in tissue repair. Excessive deposition of ECM components can lead to tissue fibrosis and dysfunction. Therefore, inhibiting the contractile function of fibroblasts is crucial for preventing fibrosis. The results of the collagen contraction assay, as shown in Fig. 2E, revealed that the collagen area in the RAP group was notably larger than that in the TGF-β1 group after 4 h. The collagen area was decreased by 39.3 % and 23.1 % in the TGF-β1 group and RAP group, respectively, compared with the initial gel area, and these differences were statistically significant (Fig. 2F). This result suggested that RAP effectively limited collagen contraction.

Cell migration is also a crucial step in tissue repair and healing processes. The results of the cell migration assay, as shown in Fig. 2G, revealed that the number of migrated cells in the RAP group was notably lower than that in the TGF-β1 group. In addition, RAP (0.5, 1, 2 and 4 μg/mL) effectively inhibited the migration of TGF-β1-activated HPFs in a concentration-dependent manner (Fig. 2H). Previous studies have shown that RAP can inhibit pulmonary fibrosis by inhibiting the proliferation, contraction and migration of lung fibroblasts [37,38]. In this work, we found that RAP markedly suppressed the proliferation, contraction and migration of TGF-β1-activated HPFs, possibly constituting a key mechanism underlying its anti-SCF effects.

3.4. Identification of the targets of RAP via RNA-seq analysis

The aforementioned experiments demonstrated that RAP may inhibit fibrosis by suppressing the proliferation, contraction and migration of HPFs, but the underlying molecular mechanism remains unclear. We compared the transcriptome of TGF-β1-stimulated HPFs by RNA-seq analysis to explore the molecular mechanism by which RAP inhibits fibrosis. A total of 465 genes were upregulated, and 1294 genes were downregulated in the RAP group compared with the TGF-β1 group (Fig. 3A).

The differentially expressed genes were visualized in volcano plots (Fig. 3B) and heatmaps (Fig. 3C). According to the results of the Gene Ontology (GO) enrichment analysis, RAP dramatically affected the expression of genes related to the regulation of the cytoplasm, ECM, and collagen-containing ECM in the cellular component category (Fig. 3D). KEGG enrichment analysis revealed that signaling pathways associated with the PI3K/AKT signaling pathway were significantly enriched in the differentially expressed genes (Fig. 3E). This finding implies that RAP might exert its effects through the PI3K/AKT signaling pathway.

3.5. RAP induces autophagy and inhibits HPFs activation by modulating the activity of the PI3K/AKT/mTORC1/WIPI2 signaling pathway

Hyperactive HPFs secrete large amounts of ECM components,

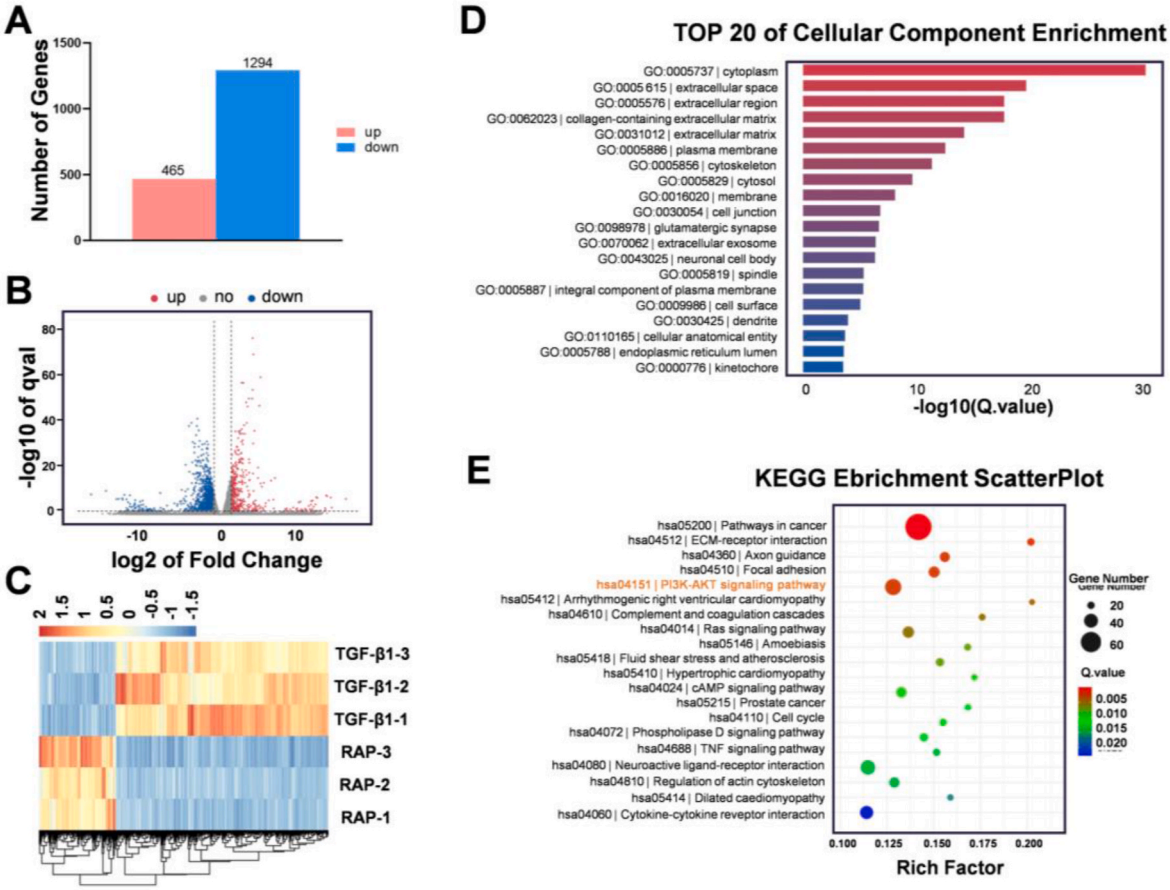

Fig. 3. The effect of RAP on HPFs is associated with the PI3K-AKT signaling pathway. (A) Numbers of differentially expressed genes. Volcano plot (B) and heatmap (C) of the differentially expressed genes. (D) Histogram showing the results of the GO enrichment analysis of the differentially expressed genes. (E) KEGG enrichment analysis of the differentially expressed genes in HPFs activated by TGF-β1(n = 3).

leading to fibrosis progression and impaired organ function. Our previous studies demonstrated that inducing autophagy can inhibit SCF [6]. LC3A and LC3B are key proteins associated with autophagosome formation. WIPI2, a crucial molecule in autophagy, participates in the formation of autophagosome membranes and autophagosomes, and after its phosphorylation, it is degraded *via* the ubiquitin ligases HECT, UBA and WWE domain containing 1 (HUWE1) [39]. Immunofluorescence analysis revealed that the expression of LC3A, LC3B and WIPI2 was significantly increased and that the expression of HUWE1 was decreased in the TGF-β1-stimulated HPFs treated with RAP (Fig. 4A and B). These results suggested that the promoting effect of RAP on cellular autophagy may be achieved through the regulation of WIPI2 signaling. The results of the western blot analysis were consistent with those of the immunofluorescence analysis. In addition to the aforementioned proteins LC3A, LC3B and WIPI2, SQSTM1/P62 also serves as a marker for autophagic activity. The expression of P62, an adapter protein in the autophagy pathway, was negatively correlated with autophagic activity [40].

Western blot analysis revealed that RAP increased the protein levels of LC3A, LC3B, and WIPI2 in the TGF-β1-stimulated HPFs while reducing the protein levels of P62, p-WIPI2, and HUWE1 (Fig. 4C and D). These results validated the ability of RAP to promote autophagy at the translational level. Furthermore, we assessed the expression of proteins associated with HPF activation, including TGF-β1, α-SMA, COL I, COL III and FN. The expression levels of these proteins decreased significantly after RAP incubation. Moreover, western blot analysis revealed decreases in the expression of the activation-related factors COL I and FN in HPFs, indicating that RAP inhibits the activation of HPFs. These results suggest that RAP can suppress HPF activation induced by TGF-β1 by inducing autophagy.

According to the RNA-seq analysis results, the PI3K/AKT signaling pathway is a potential key pathway through which RAP may exert its effects. The PI3K/AKT/mTOR signaling pathway negatively regulates autophagy and is subject to modulation by various factors [41]. RPS6 is an important substrate of mTORC1 and can positively modulate the level of mTORC1 [42]. Deptor negatively modulates mTOR activity by forming a complex with mTORC1 [43]. It is widely acknowledged that RAP is a classical inhibitor of mTOR and can inhibit its expression at multiple nodes [44]. Immunofluorescence analysis revealed significant reductions in the protein levels of mTOR and p-mTOR in the RAP group compared with both the TGF-β1 group and the CON group. Additionally, the mean fluorescence intensities of PI3K, p-PI3K, AKT1, AKT1/2/3, p-AKT, RPS6, p-RPS6 and Deptor were decreased in the RAP group (Fig. 5A and B). These results indicate that RAP modulates mTOR through the aforementioned factors. Research has shown that mTOR can control the degradation of WIPI2 through HUWE1 to regulate autophagy, establishing a link between mTOR and autophagy [45]. The regulatory associated protein of mTOR (Raptor), a principal structural component of the mTORC1 complex, positively regulates mTOR [46]. Western blot analysis revealed that RAP suppressed mTOR expression and decreased the protein levels of PI3K, p-PI3K, AKT1, AKT1/2/3, p-AKT, RPS6, p-RPS6 and Raptor(Fig. 5C and D). These results confirmed that RAP induces autophagy by modulating the PI3K/AKT/mTORC1 signaling pathway at the cellular and translational levels. In summary, RAP induces autophagy and inhibits HPFs activation by modulating the PI3K/AKT/mTORC1/WIPI2 signaling pathway. CP/RAP was consistent with the results of the drug, increasing autophagy levels and modulating mTOR and antifibrotic effects (Fig. S2).

3.6. RAP inhibits SCF in vivo by promoting autophagy

Subconjunctival injury and repair are complex pathophysiological processes that encompass four stages—hemostasis, inflammation, proliferation, and tissue remodeling—and involve multiple effector cells [7]. We successfully established a rat subconjunctival injury model by isolating subconjunctival tissue [6,47]. By modulating the mTOR pathway, RAP exerts a range of pharmacological effects, such as immunosuppressive, anticancer, anti-inflammatory, antiaging, and anti-fibrotic effects [48–50]. In this study, we used a RAP-loaded self--healing hydrogel to treat subconjunctival injury in rats and scored the effect of the treatment on SCF at weeks 2 and 8 based on established criteria (Fig. 6A, Table S1).

Two weeks postsurgery, slit lamp observation revealed conjunctival congestion and edema in the CON and CP groups (Fig. 6B and C), and H&E staining revealed substantial infiltration of inflammatory cells (Fig. 6D). However, the number of inflammatory cells was markedly reduced in the CP/RAP group. At 8 weeks after surgery, the conjunctival tissues in all of the groups presented no notable indications of congestion, edema, or inflammatory infiltration. To further investigate whether CP/RAP facilitates autophagy *in vivo*, immunofluorescence staining of LC3A and LC3B (Fig. 7A and B) was conducted on conjunctival tissues from each group. Compared with the CON and CP groups, the CP/RAP group presented increased expression of LC3A and LC3B at 2 weeks after surgery (Fig. 7C). We conducted additional investigations to determine whether the promotion of autophagy has an inhibitory effect on subconjunctival fibrosis. Masson staining (Fig. 7D) and immunofluorescence staining (Fig. 7E, F and G) were used for validation. RAP significantly inhibited collagen synthesis and decreased the expression of COL I, COL III, and FN at 8 weeks (Fig. 7H). In brief, these results indicated that RAP effectively promoted autophagy and inhibited SCF.

3.7. CP/RAP exhibits excellent biocompatibility

To assess the long-term effects of this system on ocular tissues following subconjunctival placement, evaluations of anterior and posterior segment images, intraocular pressure (IOP), immunohistochemistry, and immunofluorescence were conducted at 8 weeks postoperatively. Images of the anterior segment and fluorescein sodium staining of the cornea indicated no signs of corneal epithelial damage or cataract formation in any group (Fig. S3). Fundus and optical coherence tomography (OCT) images revealed no differences among groups, and no retinal abnormalities were observed (Fig. S4). Compared with those of normal rats, IOP measurements also showed no increase in any group relative to normal rats (Fig. S5). H&E staining of ocular tissues indicated no pathological changes in the cornea, iris, or retina (Fig. S6). TUNEL staining further confirmed the absence of apoptotic cells in the cornea and retina across all groups (Fig. S7). Collectively, these findings demonstrate that the hydrogel system exhibits excellent biocompatibility.

In this work, an injectable shape-adaptive hydrogel system with permanent release of RAP was designed. The self-healing ability and excellent biocompatibility of this system make it a potential therapeutic platform that can be conveniently injected into sites of injury. The system achieved *in situ* sustained release of RAP to interfere with SCF, overcoming the current challenges of low drug bioavailability and frequent administration and thus significantly improving patient compliance.

Safety evaluations of this system revealed no increase in IOP two months after CP/RAP subconjunctival implantation, and slit-lamp examinations showed no corneal epithelial damage. OCT imaging demonstrated no differences between groups and no abnormalities in the retina. Furthermore, histological analysis indicated no significant pathological changes in the cornea, iris, lens, or retina, while TUNEL staining confirmed the absence of apoptosis in these tissues. *In vitro* safety assessments showed that the system had no notable impact on HPFs viability. Thus, CP/RAP effectively mitigates the issues of increased IOP, corneal toxicity, and scleral melting commonly associated with glucocorticoids, NSAIDs, and MMC [7–9]. Moreover, the single intraoperative application of CP/RAP avoids the need for multiple invasive subconjunctival injections of 5-FU, demonstrating a safe and effective antifibrotic effect [10].

Subconjunctival fibrosis plays a crucial role in the progression of

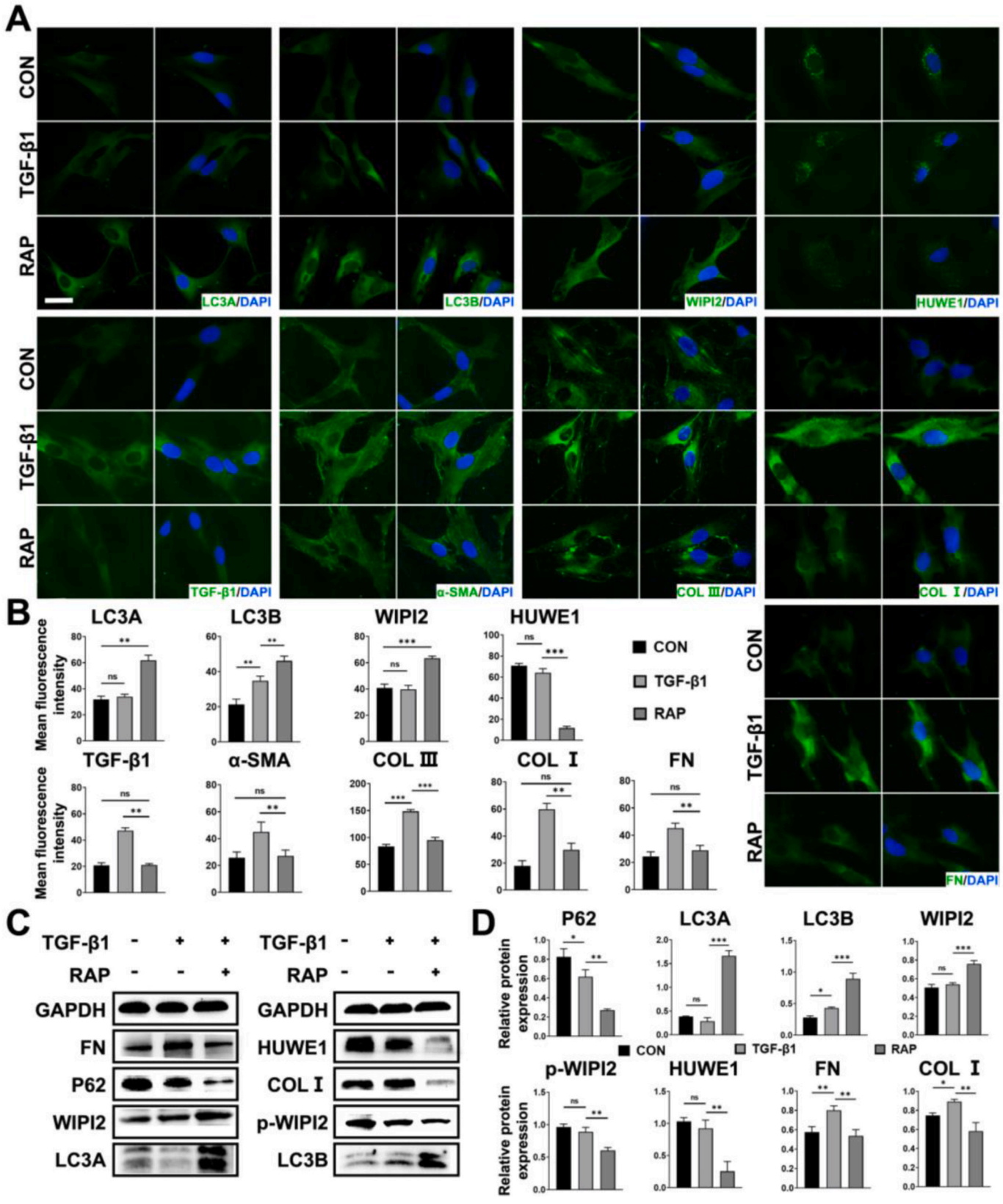

Fig. 4. RAP promotes autophagy and inhibits HPFs activation. Representative immunofluorescence images (A) and semiquantitative analysis (B) of autophagy-related proteins and activation-related proteins in HPFs (n = 5). Representative western blot images (C) and statistical analysis (D) of the expression of proteins (n = 3). *Scale bar*: 150 μm. *Error bars*: 95 % CI. $^{*}P < 0.05$, $^{**}P < 0.01$, $^{***}P < 0.001$.

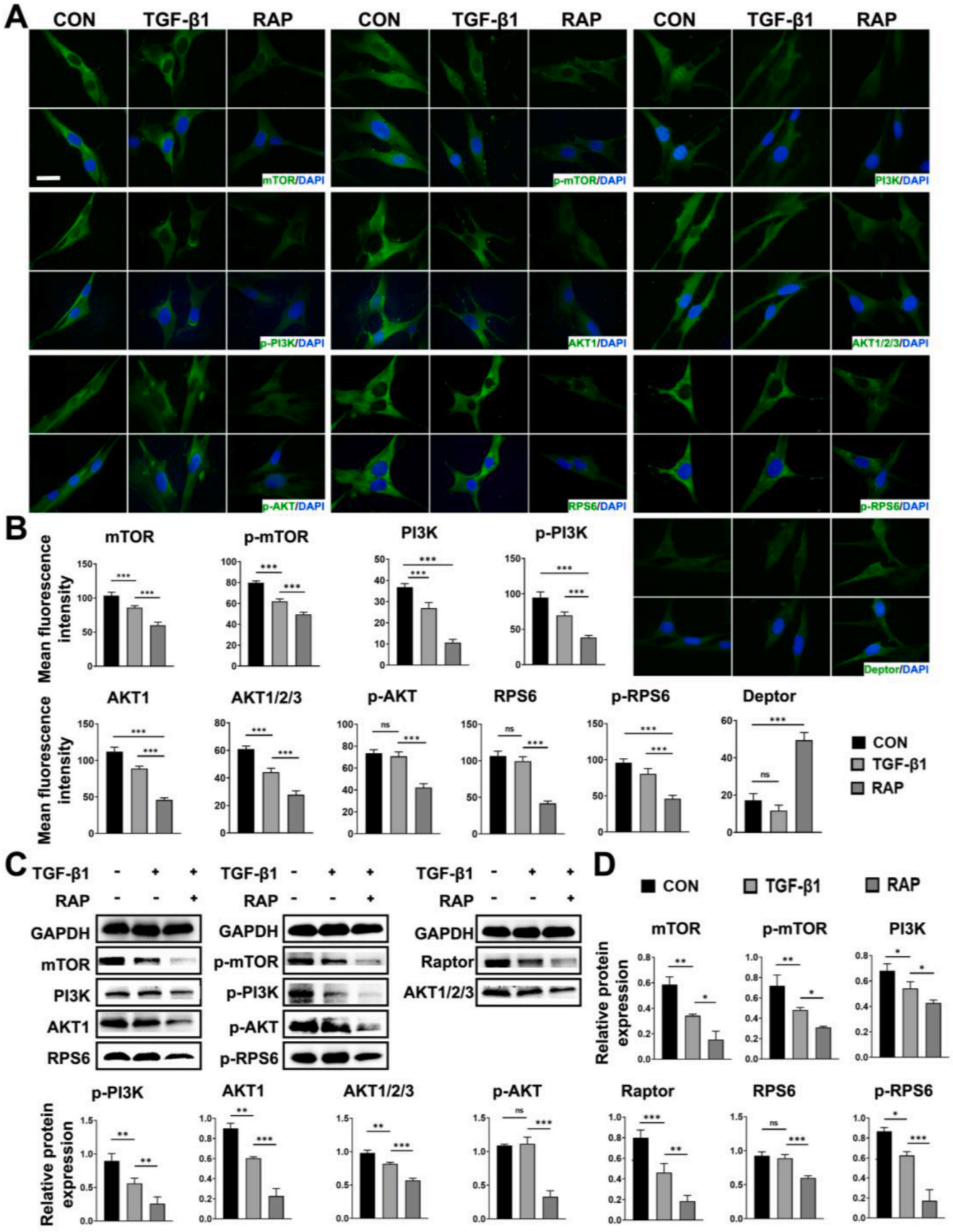

Fig. 5. RAP inhibits mTOR expression by modulating the PI3K/AKT pathway. Representative immunofluorescence images (A) and semiquantitative analysis (B) of PI3K/AKT/mTOR pathway protein and regulatory protein expression in HPFs (n = 5). Representative western blot images (C) and statistical analysis (D) of the expression of proteins (n = 3). *Scale bar*: 150 μm. *Error bars*: 95 % CI. $^{*}P < 0.05$, $^{**}P < 0.01$, $^{***}P < 0.001$.

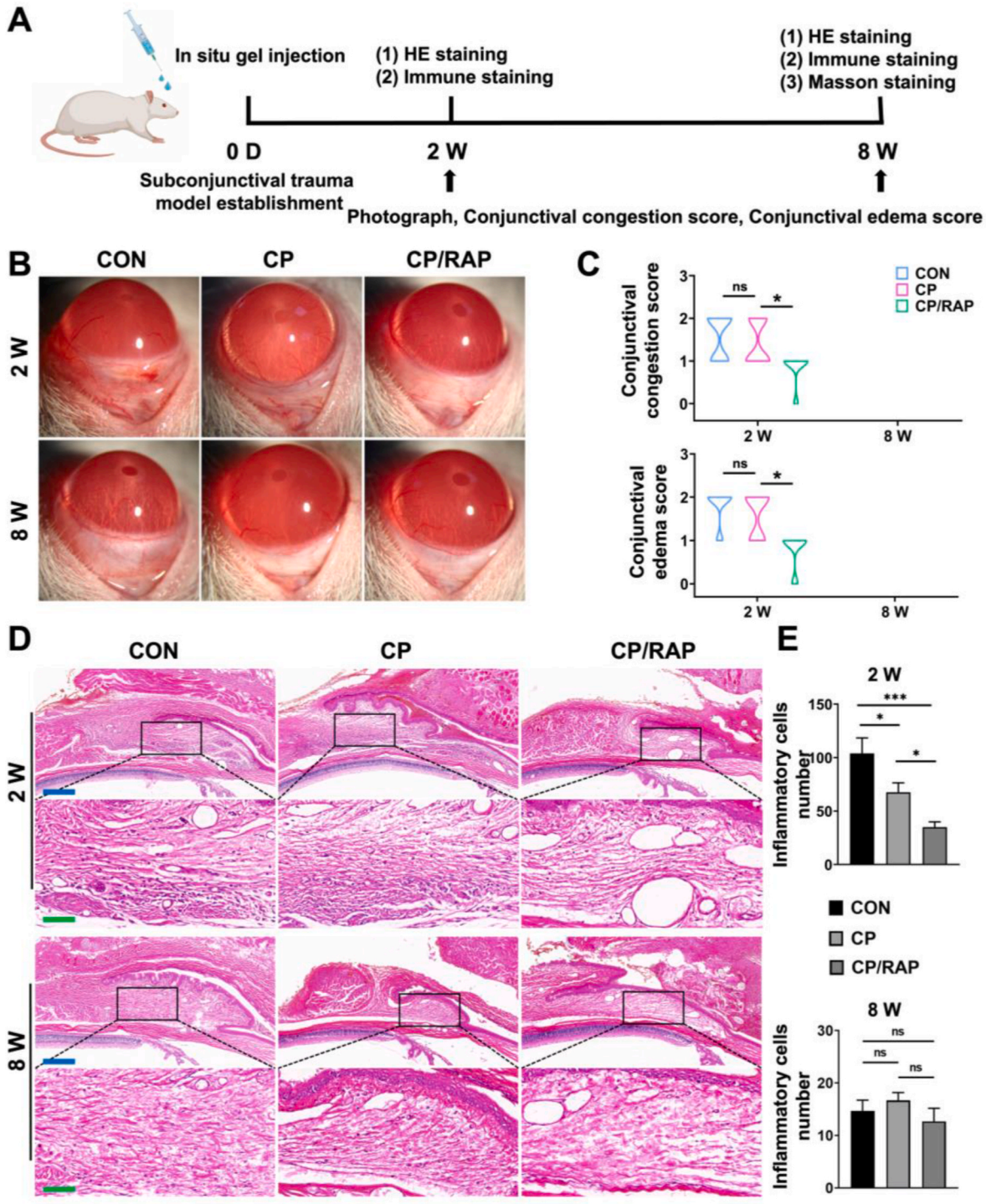

Fig. 6. RAP inhibits conjunctival inflammation at 2 weeks. Establishment of and treatment schedule for a rat model of subconjunctival injury (A). Postoperative representative images (B) and scores (C) of the rats (n = 5). (D) H&E staining. (E) Statistical analysis of infiltrating inflammatory cells (n = 3). Blue scale bar: 400 μm, green scale bar: 100 μm. *Error bars*: 95 % CI. $^{*}P < 0.05$, $^{**}P < 0.01$, $^{***}P < 0.001$. (For interpretation of the references to color in this figure legend, the reader is referred to the Web version of this article.)

numerous diseases. Local application of RAP can promote autophagy and inhibit fibroblast activation, thereby suppressing fibrosis. However, its low water solubility and the presence of ocular barriers pose challenges to its bioavailability [51]. The present research revealed that subconjunctival injection of a hydrogel drug delivery system facilitates the uninterrupted release of drugs, consequently substantially increasing the therapeutic efficacy of drugs for ocular diseases [28–30]. Hence, the formulation of a hydrogel system for the sustained delivery of RAP to alleviate subconjunctival fibrosis and enable drug administration during surgery could be a viable alternative.

The progressive development of SCF is closely associated with the sustained activation of HPFs. TGF-β1 is the primary cytokine that promotes fibrosis and activates the Smad 2/3 signaling pathway by binding to TGF-βRII. This process promotes the activation of myofibroblasts, resulting in ECM deposition [52]. This study revealed that RAP at a concentration of 2 μg/mL inhibited the proliferation, contraction, and

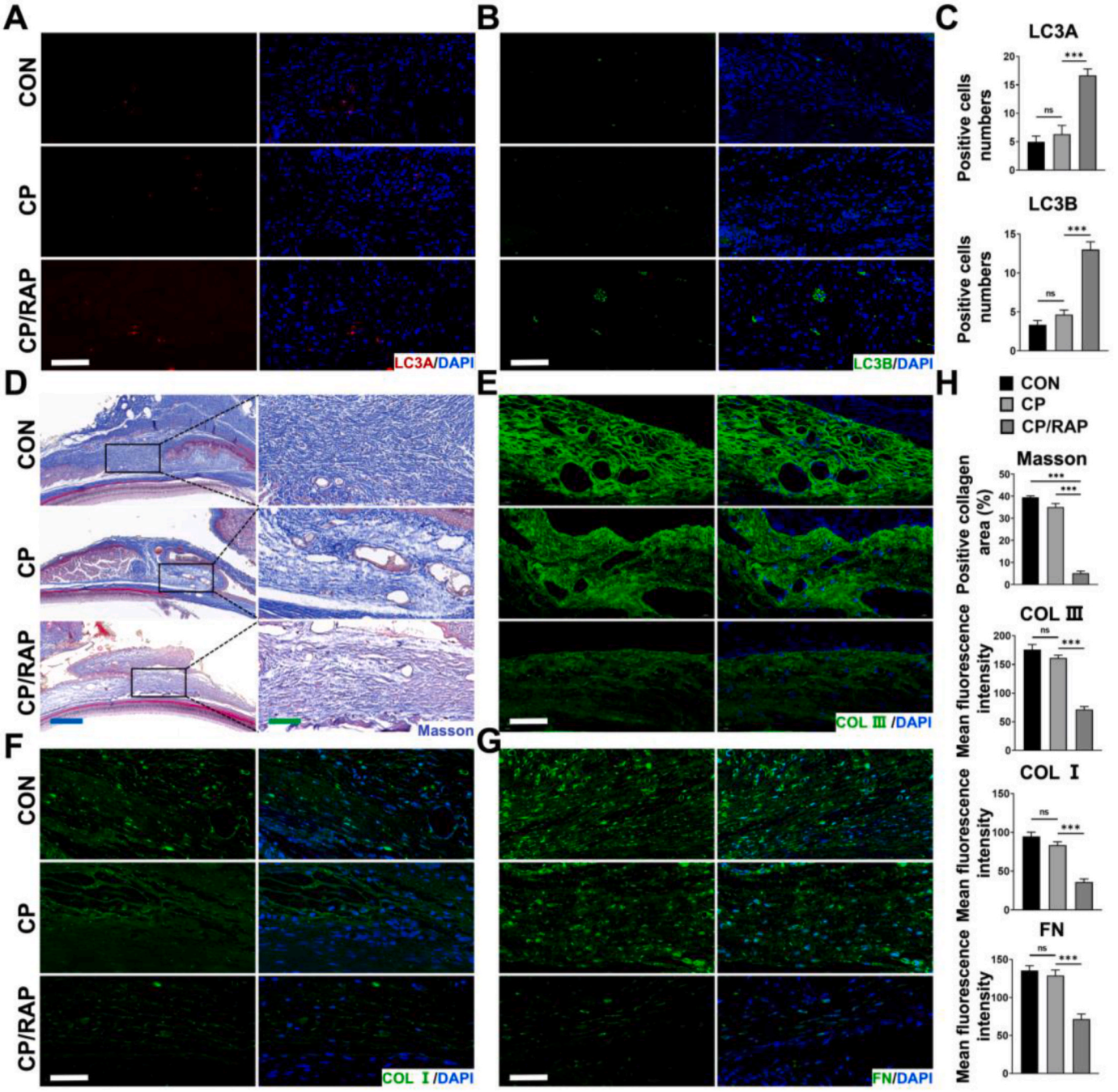

Fig. 7. RAP promotes autophagy to inhibit SCF. LC3A (A) and LC3B (B) staining at 2 postoperative weeks and statistical analysis of the data (n = 3) (C). Masson (D), COL III (E), COL I (F) and FN (G) staining. (H) Statistical analysis of the positive collagen area and fluorescence intensity (n = 3). *White scale bar:* 50 μm, *blue scale bar:* 400 μm, *green scale bar*: 100 μm. *Error bars*: 95 % CI. $^{*}P < 0.05$, $^{**}P < 0.01$, $^{***}P < 0.001$. (For interpretation of the references to color in this figure legend, the reader is referred to the Web version of this article.)

migration of HPFs activated by TGF-β1, indicating its potential therapeutic effects on SCF.

We speculated that autophagy may play an important role in inhibiting fibrosis, potentially through mechanisms associated with the PI3K/AKT/mTOR signaling pathway. We demonstrated that after treatment with RAP, the protein levels of LC3A and LC3B and those of FN, COL I, and COL III were decreased in rat tissues, suggesting that RAP may inhibit SCF by promoting autophagy.

mTOR is a crucial node in autophagy regulation. Accumulating evidence indicates that mTOR plays a negative regulatory role in autophagy [53]. RNA-seq revealed enrichment of the PI3K/AKT pathway, an upstream regulatory pathway of mTOR, following RAP treatment. Furthermore, the regulation of mTOR by Deptor and Raptor, which function as negative and positive regulatory factors upstream of mTOR, respectively, has been confirmed at both the cellular and translational levels. mTOR can also regulate autophagy by promoting the degradation of WIPI2, which was confirmed in our study. In summary, RAP inhibited the PI3K/AKT pathway in HPFs, promoted the expression of Deptor and WIPI2, and inhibited the expression of Raptor. Taken together, these findings indicate that RAP mediates autophagy inhibition to mitigate SCF through the regulation of mTOR.

4. Conclusion

In conclusion, a self-adaptive hydrogel system with *in situ* sustained release of RAP was designed and applied to interfere with SCF. The system exhibited moderate mechanical properties, along with injectability, degradability, biocompatibility and safety. When this system was used to treat subconjunctival trauma, collagen levels and ECM component deposition were decreased, and scar formation was inhibited. The *in vivo* and *in vitro* results indicated that autophagy mediated *via* the PI3K/AKT/mTOR/WIPI2 signaling pathway inhibits SCF and that mTOR modulation plays a critical role in this process. This system provides a novel therapeutic approach and potential molecular mechanism for SCF, which may offer insights useful for the treatment of other fibrotic ophthalmological diseases.

CRediT authorship contribution statement

Xue Sun: Writing – original draft, Software, Resources, Investigation, Formal analysis, Data curation. **Haohao Cui:** Writing – original draft, Software, Methodology, Investigation. **Jingfan Li:** Software, Investigation. **Boyuan An:** Software, Investigation. **Ruixing Liu:** Investigation, Funding acquisition, Conceptualization. **Zhihua Guo:** Software, Methodology. **Dandan Chu:** Software, Methodology. **Xingchen Geng:** Software, Investigation. **Bingbing Cui:** Software, Methodology, Investigation. **Lei Zhu:** Supervision, Methodology. **Jingguo Li:** Writing – review & editing, Supervision, Resources, Project administration, Funding acquisition, Conceptualization. **Zhanrong Li:** Writing – review & editing, Visualization, Validation, Supervision, Software, Project administration, Funding acquisition, Data curation, Conceptualization.

Declaration of competing interest

The authors declare that they have no known competing financial interests or personal relationships that could have appeared to influence the work reported in this paper.

Acknowledgements

This research was supported by the National Natural Science Foundation of China, China (82371108, 52173143 and 82101090), the Natural Science Foundation of Henan Province, China (242300421018) Henan Province Science and Technology Research and Development Plan Joint Fund Project, China (242301420010), Henan Province Youth Health Science and Technology Innovation Talent Training Project, China (LJRC2024003) and the Basic Science Key Project of Henan Eye Hospital, China (22JCQN001 and 23JCZD001).

Appendix A. Supplementary data

Supplementary data to this article can be found online at https://doi.org/10.1016/j.mtbio.2024.101380.

Data availability

No data was used for the research described in the article.

References

[1] C. Lan, J. Tan, L. Tang, G. Liu, L. Huang, X. Luo, L. Zhou, Y. Zhu, X. Liu, N. Fan, Forkhead domain inhibitory-6 attenuates subconjunctival fibrosis in rabbit model with trabeculectomy, Exp. Eye Res. 210 (2021) 108725, https://doi.org/10.1016/j.exer.2021.108725.

[2] J. Shu, L. Hu, Y. Wu, L. Chen, K. Huang, Z. Wang, M. Liang, Daidzein suppresses TGF-β1-induced cardiac fibroblast activation via the TGF-β1/SMAD2/3 signaling pathway, Eur. J. Pharmacol. 919 (2022) 174805, https://doi.org/10.1016/j.ejphar.2022.174805.

[3] D. Kong, Z. Zhang, L. Chen, W. Huang, F. Zhang, L. Wang, Y. Wang, P. Cao, S. Zheng, Curcumin blunts epithelial-mesenchymal transition of hepatocytes to alleviate hepatic fibrosis through regulating oxidative stress and autophagy, Redox Biol. 36 (2020) 101600, https://doi.org/10.1016/j.redox.2020.101600.

[4] Y. Ding, Sl Kim, S.Y. Lee, J.K. Koo, Z. Wang, M.E. Choi, Autophagy regulates TGF-β expression and suppresses kidney fibrosis induced by unilateral ureteral obstruction, J. Am. Soc. Nephrol. 25 (2014) 2835–2846, https://doi.org/10.1681/ASN.2013101068.

[5] J. Zhang, H. Wang, H. Chen, H. Li, P. Xu, B. Liu, Q. Zhang, C. Lv, X. Song, ATF3-activated accelerating effect of LINC00941/lncIAPF on fibroblast-to-myofibroblast differentiation by blocking autophagy depending on ELAVL1/HuR in pulmonary fibrosis, Autophagy 18 (2022) 2636–2655, https://doi.org/10.1080/15548627.2022.2046448.

[6] Z. Li, Z. Guo, D. Chu, R. Liu, L. Zhu, L. Shi, C. Li, L. Jin, X. Zhang, J. Li, Celastrol-based nanoporous membranes prevent subconjunctival fibrosis by activating autophagy, Mater Today Adv 15 (2023) 1000356, https://doi.org/10.1016/j.mtadv.2023.100356.

[7] M. Zada, U. Pattamatta, A. White, Modulation of fibroblasts in conjunctival wound healing, Ophthalmology 125 (2018) 179–192, https://doi.org/10.1016/j.ophtha.2017.08.028.

[8] R. Sun, S. Ma, X. Chen, Y. Deng, J. Gou, T. Yin, H. He, Y. Wang, X. Tang, Y. Zhang, Inflammation-responsive molecular-gated contact lens for the treatment of corneal neovascularization, J. Contr. Release 360 (2023) 818–830, https://doi.org/10.1016/j.jconrel.2023.07.036.

[9] K. Bell, Bezerra B. de Padua Soares, M. Mofokeng, G. Montesano, M.E. Nongpiur, M.V. Marti, M. Lawlor, Learning from the past: mitomycin C use in trabeculectomy and its application in bleb-forming minimally invasive glaucoma surgery, Surv. Ophthalmol. 66 (2021) 109–123, https://doi.org/10.1016/j.survophthal.2020.05.005.

[10] J. Swogger, I.P. Conner, C. Happ-Smith, M.C. Kemmerer, D.R. Julian, R. Davis, A. Wells, J.S. Schuman, C.C. Yates, Novel combination therapy reduces subconjunctival fibrosis after glaucoma filtration surgery in the rabbit model, Clin. Exp. Ophthalmol. 49 (2021) 60–69, https://doi.org/10.1111/ceo.13884.

[11] E.G. Foerster, T. Mukherjee, L. Cabral-Fernandes, J.D.B. Rocha, S.E. Girardin, D. J. Philpott, How autophagy controls the intestinal epithelial barrier, Autophagy 18 (2022) 86–103, https://doi.org/10.1080/15548627.2021.1909406.

[12] S. Swaminathan, J.L. Arbiser, K.M. Hiatt, W. High, S. Abul-Ezz, T.D. Horn, S. V. Shah, Rapid improvement of nephrogenic systemic fibrosis with rapamycin therapy: possible role of phospho-70-ribosomal-S6 kinase, J. Am. Acad. Dermatol. 62 (2010) 343–345, https://doi.org/10.1016/j.jaad.2009.04.022.

[13] M. Wijesinha, J.M. Hirshon, M. Terrin, L. Magder, C. Brown, K. Stafford, A. Iacono, Survival associated with sirolimus plus tacrolimus maintenance without induction therapy compared with standard immunosuppression after lung transplant, JAMA Netw. Open 2 (2019) e1910297, https://doi.org/10.1001/jamanetworkopen.2019.10297.

[14] W. Fan, H. Han, Y. Chen, X. Zhang, Y. Gao, S. Li, Q. Jin, J. Ji, K. Yao, Antimicrobial nanomedicine for ocular bacterial and fungal infection, Drug Deliv Transl Res 11 (2021) 1352–1375, https://doi.org/10.1007/s13346-021-00966-x.

[15] K. Voss, K. Falke, A. Bernsdorf, N. Grabow, C. Kastner, K. Sternberg, I. Minrath, T. Eickner, A. Wree, K.P. Schmitz, R. Guthoff, M. Witt, M. Hovakimyan, Development of a novel injectable drug delivery system for subconjunctival glaucoma treatment, J. Contr. Release 214 (2015) 1–11, https://doi.org/10.1016/j.jconrel.2015.06.035.

[16] M. Matsuzawa, T. Ando, S. Fukase, M. Kimura, Y. Kume, T. Ide, K. Izawa, A. Kaitani, M. Hara, E. Nakamura, A. Kamei, A. Matsuda, N. Nakano, K. Maeda, N. Tada, H. Ogawa, K. Okumura, A. Murakami, N. Ebihara, J. Kitaura, The protective role of conjunctival goblet cell mucin sialylation, Nat. Commun. 14 (2023) 1417, https://doi.org/10.1038/s41467-023-37101-y.

[17] R. Rong, X. Zhou, G. Liang, H. Li, M. You, Z. Liang, Z. Zeng, H. Xiao, D. Ji, X. Xia, Targeting Cell Membranes, Depleting ROS by dithiane and thioketal-containing polymers with pendant cholesterols delivering necrostatin-1 for glaucoma treatment, ACS Nano 16 (2022) 21225–21239, https://doi.org/10.1021/acsnano.2c09202.

[18] F. Zhang, M. Lv, S. Wang, M. Li, Y. Wang, C. Hu, W. Hu, X. Wang, X. Wang, Z. Liu, Z. Fan, J. Du, Y. Sun, Ultrasound-triggered biomimetic ultrashort peptide nanofiber hydrogels promote bone regeneration by modulating macrophage and the osteogenic immune microenvironment, Bioact. Mater. 31 (2023) 231–246, https://doi.org/10.1016/j.bioactmat.2023.08.008.

[19] F. Wang, H. Su, Z. Wang, C.F. Anderson, X. Sun, H. Wang, P. Laffont, J. Hanes, H. Cui, Supramolecular filament hydrogel as a universal immunomodulator carrier for immunotherapy combinations, ACS Nano 17 (2023) 10651–10664, https://doi.org/10.1021/acsnano.3c01748.

[20] C. Zou, J. Hu, D. Lu, Q. Li, Y. Jiang, R. Wang, H. Wang, X. Lei, J. Li-Ling, H. Yang, H. Xie, A self-fused hydrogel for the treatment of glottic insufficiency through outstanding durability, extracellular matrix-inducing bioactivity and function preservation, Bioact. Mater. 24 (2022) 54–68, https://doi.org/10.1016/j.bioactmat.2022.12.006.

[21] T. Lin, W. Wang, T. Chen, B. Bao, T. Liu, H. Zhao, C. Feng, Q. Lin, L. Zhu, L. Gong, A lacrimal duct drug delivery system based on photo-induced hydrogel for dry eye and allergic conjunctivitis therapy, Composites B 266 (2023) 111014, https://doi.org/10.1016/j.compositesb.2023.111014.

[22] S. Wang, B. Chen, L. Ouyang, D. Wang, J. Tan, Y. Qiao, S. Ge, J. Ruan, A. Zhuang, X. Liu, R. Jia, A novel stimuli-responsive injectable antibacterial hydrogel to achieve synergetic photothermal/gene-targeted therapy towards uveal melanoma, Adv. Sci. 8 (2021) e2004721, https://doi.org/10.1002/advs.202004721.

[23] H. Ren, Z. Zhang, X. Cheng, Z. Zou, X. Chen, C. He, Injectable, self-healing hydrogel adhesives with firm tissue adhesion and on-demand biodegradation for sutureless wound closure, Sci. Adv. 9 (2023) eadh4327, https://doi.org/10.1126/sciadv.adh4327.
[24] P. Bertsch, M. Diba, D.J. Mooney, S.C.G. Leeuwenburgh, Self-Healing injectable hydrogels for tissue regeneration, Chem. Rev. 123 (2023) 834–873, https://doi.org/10.1021/acs.chemrev.2c00179.
[25] L. Qiao, Y. Liang, J. Chen, Y. Huang, S.A. Alsareii, A.M. Alamri, F.A. Harraz, B. Guo, Antibacterial conductive self-healing hydrogel wound dressing with dual dynamic bonds promotes infected wound healing, Bioact. Mater. 30 (2023) 129–141, https://doi.org/10.1016/j.bioactmat.2023.07.015.
[26] J. Chen, H. Zhu, Y. Zhu, C. Zhao, S. Wang, Y. Zheng, Z. Xie, Y. Jin, H. Song, L. Yang, J. Zhang, J. Dai, Z. Hu, H. Wang, Injectable self-healing hydrogel with siRNA delivery property for sustained STING silencing and enhanced therapy of intervertebral disc degeneration, Bioact. Mater. 9 (2021) 29–43, https://doi.org/10.1016/j.bioactmat.2021.08.003.
[27] Y. Yang, J. Wang, S. Huang, M. Li, J. Chen, D. Pei, Z. Tang, B. Guo, Bacteria-responsive programmed self-activating antibacterial hydrogel to remodel regeneration microenvironment for infected wound healing, Natl. Sci. Rev. 11 (2024) nwae044, https://doi.org/10.1093/nsr/nwae044.
[28] G.P. Misra, R.S. Singh, T.S. Aleman, S.G. Jacobson, T.W. Gardner, T.L. Lowe, Subconjunctivally implantable hydrogels with degradable and thermoresponsive properties for sustained release of insulin to the retina, Biomaterials 30 (33) (2009) 6541–6547, https://doi.org/10.1016/j.biomaterials.2009.08.025.
[29] Z. Shi, S.K. Li, P. Charoenputtakun, C.Y. Liu, D. Jasinski, P. Guo, RNA nanoparticle distribution and clearance in the eye after subconjunctival injection with and without thermosensitive hydrogels, J. Contr. Release 270 (2018) 14–22, https://doi.org/10.1016/j.jconrel.2017.11.028.
[30] U. Soiberman, S.P. Kambhampati, T. Wu, M.K. Mishra, Y. Oh, R. Sharma, J. Wang, A.E. Al Towerki, S. Yiu, W.J. Stark, R.M. Kannan, Subconjunctival injectable dendrimer-dexamethasone gel for the treatment of corneal inflammation, Biomaterials 125 (2017) 38–53, https://doi.org/10.1016/j.biomaterials.2017.02.016.
[31] Y. Lin, W. Luo, B. Jiang, Q. Lin, M. Tang, X. Li, L. Xie, The effect of GelDex-S58 hydrogel on anti-conjunctival scarring after glaucoma filtration surgery, iScience 26 (9) (2023) 107633, https://doi.org/10.1016/j.isci.2023.107633.
[32] J. Liu, Y. Huang, W. Yang, X. Sun, Y. Xu, Y. Peng, W. Song, J. Yuan, L. Ren, Sutureless transplantation using a semi-interpenetrating polymer network bioadhesive for ocular surface reconstruction, Acta Biomater. 153 (2022) 273–286, https://doi.org/10.1016/j.actbio.2022.09.049.
[33] L. Shi, Z. Li, Z. Liang, J. Zhang, R. Liu, D. Chu, L. Han, L. Zhu, J. Shen, J. Li, A dual-functional chitosan derivative platform for fungal keratitis, Carbohydr. Polym. 275 (2022) 118762, https://doi.org/10.1016/j.carbpol.2021.118762.
[34] N.C. Henderson, F. Rieder, T.A. Wynn, Fibrosis: from mechanisms to medicines, Nature 587 (2020) 555–566, https://doi.org/10.1038/s41586-020-2938-9.
[35] Y. Okada, K. Shirai, P.S. Reinach, A. Kitano-Izutani, M. Miyajima, K.C. Flanders, J. V. Jester, M. Tominaga, S. Saika, TRPA1 is required for TGF-β signaling and its loss blocks inflammatory fibrosis in mouse corneal stroma, Lab. Invest. 94 (2014) 1030–1041, https://doi.org/10.1038/labinvest.2014.85.
[36] M. Sobecki, K. Mrouj, A. Camasses, N. Parisis, E. Nicolas, D. Llères, F. Gerbe, S. Prieto, L. Krasinska, A. David, M. Eguren, M.C. Birling, S. Urbach, S. Hem, J. Déjardin, M. Malumbres, P. Jay, V. Dulic, DLj Lafontaine, R. Feil, D. Fisher, The cell proliferation antigen Ki-67 organises heterochromatin, Elife 5 (2016) e13722, https://doi.org/10.7554/eLife.13722.
[37] W. Tai, S. Deng, W. Wu, Z. Li, W. Lei, Y. Wang, C. Vongphouttha, T. Zhang, Z. Dong, Rapamycin attenuates the paraquat-induced pulmonary fibrosis through activating Nrf2 pathway, J. Cell. Physiol. 235 (2020) 1759–1768, https://doi.org/10.1002/jcp.29094.
[38] E.J. Chung, A. Sowers, A. Thetford, G. McKay-Corkum, S.I. Chung, J.B. Mitchell, D. E. Citrin, Mammalian target of rapamycin inhibition with rapamycin mitigates radiation-induced pulmonary fibrosis in a murine model, Int. J. Radiat. Oncol. Biol. Phys. 96 (2016) 857–866, https://doi.org/10.1016/j.ijrobp.2016.07.026.
[39] W. Wan, W. Liu, MTORC1 regulates autophagic membrane growth by targeting WIPI2, Autophagy 15 (2019) 742–743, https://doi.org/10.1080/15548627.2019.1569949.
[40] J.N.S. Vargas, M. Hamasaki, T. Kawabata, R.J. Youle, T. Yoshimori, The mechanisms and roles of selective autophagy in mammals, Nat. Rev. Mol. Cell Biol. 24 (2023) 167–185, https://doi.org/10.1038/s41580-022-00542-2.
[41] X. Wang, C. Shen, T. Wang, Y. Huang, Y. Jin, M. Zhou, M. Zhang, S. Gu, M. Wang, Z. Liu, R. Li, L. Cai, Shikonin suppresses rheumatoid arthritis by inducing apoptosis and autophagy via modulation of the AMPK/mTOR/ULK-1 signaling pathway, Phytomedicine 128 (2024) 155512, https://doi.org/10.1016/j.phymed.2024.155512.
[42] H.Y. Hwang, J.S. Shim, D. Kim, H.J. Kwon, Antidepressant drug sertraline modulates AMPK-MTOR signaling-mediated autophagy via targeting mitochondrial VDAC1 protein, Autophagy 17 (2021) 2783–2799, https://doi.org/10.1080/15548627.2020.1841953.
[43] S. Battaglioni, D. Benjamin, M. Wälchli, T. Maier, M.N. Hall, mTOR substrate phosphorylation in growth control, Cell 185 (2022) 1814–1836, https://doi.org/10.1016/j.cell.2022.04.013.
[44] J. Simcox, D.W. Lamming, The central moTOR of metabolism, Dev. Cell 57 (2022) 691–706, https://doi.org/10.1016/j.devcel.2022.02.024.
[45] W. Wan, Z. You, L. Zhou, Y. Xu, C. Peng, T. Zhou, C. Yi, Y. Shi, W. Liu, mTORC1-regulated and HUWE1-mediated WIPI2 degradation controls autophagy flux, Mol. Cell 72 (2018) 303–315.e6, https://doi.org/10.1016/j.molcel.2018.09.017.
[46] D.H. Kim, D.D. Sarbassov, S.M. Ali, J.E. King, R.R. Latek, H. Erdjument-Bromage, P. Tempst, D.M. Sabatini, mTOR interacts with raptor to form a nutrient-sensitive complex that signals to the cell growth machinery, Cell 110 (2002) 163–175, https://doi.org/10.1016/s0092-8674(02)00808-5.
[47] Z. Li, X. Zhang, Z. Guo, L. Shi, L. Jin, L. Zhu, X. Cai, J. Zhang, Y. Zhang, J. Li, Nature-derived bionanomaterials for sustained release of 5-fluorouracil to inhibit subconjunctival fibrosis, Mater Today Adv 11 (2021) 100150, https://doi.org/10.1016/j.mtadv.2021.100150.
[48] H. Querfurth, H.K. Lee, Mammalian/mechanistic target of rapamycin (mTOR) complexes in neurodegeneration, Mol. Neurodegener. 16 (2021) 44, https://doi.org/10.1186/s13024-021-00428-5.
[49] Z. Zhang, C. Shen, Q. Long, Z. Yang, R. Dai, J. Wang, W. Zhang, Q. Pan, Z. Zhu, K. Xu, Sirolimus for retinal astrocytic hamartoma associated with tuberous sclerosis complex, Ophthalmology 122 (2015) 1947–1949, https://doi.org/10.1016/j.ophtha.2015.03.023.
[50] R. Wang, J. Lu, J. Yin, H. Chen, H. Liu, F. Xu, T. Zang, R. Xu, C. Li, Y. Wu, Q. Wu, X. Fei, M. Zhu, L. Shen, J. Ge, A TEMPOL and rapamycin loaded nanofiber-covered stent favors endothelialization and mitigates neointimal hyperplasia and local inflammation, Bioact. Mater. 19 (2022) 666–677, https://doi.org/10.1016/j.bioactmat.2022.04.033.
[51] H. Chen, X. Geng, Q. Ning, L. Shi, N. Zhang, S. He, M. Zhao, J. Zhang, Z. Li, J. Shi, J. Li, Biophilic positive carbon dot exerts antifungal activity and augments corneal permeation for fungal keratitis, Nano Lett. 24 (13) (2024) 4044–4053, https://doi.org/10.1021/acs.nanolett.4c01042.
[52] R. Liu, J. Li, Z. Guo, D. Chu, C. Li, L. Shi, J. Zhang, L. Zhu, Z. Li, Celastrol alleviates corneal stromal fibrosis by inhibiting TGF-β1/Smad2/3-YAP/TAZ signaling after descemet stripping endothelial keratoplasty, Invest. Ophthalmol. Vis. Sci. 64 (2023) 9, https://doi.org/10.1167/iovs.64.3.9.
[53] Z. Li, R. Liu, X. Zhang, Z. Guo, X. Geng, D. Chu, H. Cui, A. Zhang, W. Li, L. Zhu, J. Li, An injectable thermoresponsive-hydrogel for lamellar keratoplasty: in-situ releases celastrol and hampers corneal scars, J. Contr. Release 369 (2024) 604–616, https://doi.org/10.1016/j.jconrel.2024.04.010.